



A new type of sandwich panel with periodic cellular metal cores and its mechanical performances

Chae-Hong Lim, Insu Jeon, Ki-Ju Kang*

Depart. of Mechanical Engineering, Chonnam National University, 300 Yongbongdong Bukku, Kwangju 500-757, Republic of Korea

ARTICLE INFO

Article history:

Received 29 August 2008

Accepted 2 December 2008

Available online 14 December 2008

Keywords:

Expanded-metal

Kagome truss

Sandwich panel

Ultra light metal structure

ABSTRACT

Many studies have been performed on the mechanical properties and optimization of truss PCMs (periodic cellular metals), but those on the fabrication process, which is one of key factors determining the survivability of PCMs in the market, have been relatively limited. This study introduces a new idea on the fabrication of quasi Kagome truss cored sandwich panels, which is based on the expanded-metal process. And the mechanical behavior of the sandwich panels is to be evaluated. The mechanical strengths and failure mechanisms under compression and bending load are estimated based on elementary mechanics of materials, and the optimal design is derived. Its validity is proved by comparison with the results of experiments. The results showed that the new idea is promising with respect to all three requirements, i.e., the morphology, fabrication cost, and raw materials. The simple mechanical analysis was sufficiently effective and accurate for estimating the performance and failure mode of the sandwich panels. In the experiments, sandwich panel specimens of three different designs were compared in their bending behaviors to demonstrate sensitivity of geometric parameters. Namely, although all the designs had little difference in their load capacity-per-weight, the failure mechanisms and the behaviors after a peak load were totally different.

© 2008 Elsevier Ltd. All rights reserved.

1. Introduction

Truss PCM (periodic cellular metal) was introduced in early 2000s. It has ideal mechanical properties because it consists of regular trusses [1–4]. When serving as a core of a sandwich panel subjected to bending, the truss PCM is as good as a honeycomb in terms of strength for a given weight [5,6]. The types of truss available are pyramid, octet, Kagome and so on. The octet truss is one of the most ideal trusses, because it consists of regular tetrahedrons. Kagome truss is the one introduced most recently [7]. For a given relative density, though its elastic stiffness is exactly the same as the octet truss, the length of each strut composing the Kagome truss is only half of that composing the octet truss. Consequently, its strength against elastic buckling, which is one of the major failure mechanisms of truss PCMs, can increase by up to four times of that of the octet truss, and the duplex structure (with a large parallelepiped having two small tetrahedrons at the sharp ends in the unit cell) gives advantages in terms of the efficiency in using the inner space. See Fig. 1 for a unit cell of the Kagome truss in comparison with that of the octet truss. Also, directional variance of the mechanical and physical properties, i.e., anisotropy is relatively low [7,8].

Truss PCMs can be fabricated by investment casting, laying-up of wire meshes or bending of perforated sheet [1–3,9–11], but each method has its own shortcomings such as high cost, casting defects, deterioration of the strength due to non-ideal truss structure and material loss due to the perforation. Recent works [12,13] have shown that the pyramidal truss structure can be fabricated from an expanded-metal net. This method has a great advantage over the other methods since it requires the least material loss and uses a well-established process for the expanded metals. However, its strength against elastic buckling is lower than that of Kagome truss, because struts composing the pyramidal truss are longer than those of the Kagome truss for given height of a single layered truss. Lim and Kang [14] and Kang et al. [15] have introduced new methods to fabricate the octet and Kagome trusses using wires as the raw material. These methods are based on tri-axial weaving and can use high strength metal wires as the raw material. However, there are difficulties in fabricating with thick wires due to the interference among wires when crossing each other, which may cause the deflections of the truss elements.

To evaluate the market feasibility of a truss PCM, we believe, the following three aspects should be considered;

- (i) the morphology,
- (ii) fabrication cost, and
- (iii) raw materials.

* Corresponding author. Tel.: +82 62 530 1688; fax: +82 62 530 1689.
E-mail address: kjkang@chonnam.ac.kr (K.-J. Kang).

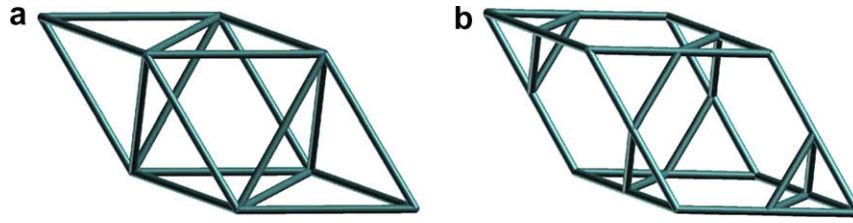


Fig. 1. Configurations of a unit cell of (a) ideal Octet truss and (b) ideal Kagome truss.

The first aspect means that the ideal types of truss, especially the Kagome truss, are preferred for its high specific strength, i.e., strength per weight. To reduce the cost, the fabrication process should be suitable for mass-production. Simple, continuous and well developed processes are required. Classical metal forming processes like press working or expanding seem promising, because the processes are well-established, which can minimize investment for developing the mass-production system. The last aspect would mean that wrought and high strength alloys should be used as raw materials. If a truss PCM is made of quenched steel or age-hardening aluminum alloy, it would be beneficial with respect to the second and last aspects. Namely, it could provide good formability in annealed state during fabrication processes as well as high material strength by heat treatment after assembly into the final shape.

If a single truss layered structure used as the core of sandwich panel is to be fabricated, among the various fabrication methods mentioned above, the one based on the expanded-metal process would be the most attractive in terms of cost and raw material. In the expanded-metal process, pattern cutting and expanding into a diamond mesh are simultaneously carried out in a single stroke of press without any material loss. Then, the mesh is just simply bent into a triangular wave pattern to be a pyramidal truss core [12,13]. However, one problem remains: How do we fabricate the Kagome truss by applying the expanded-metal process? This study intends to answer to the question by suggesting a new idea on the fabrication of a Kagome-like structure based on the expanded-metal process. The mechanical properties and failure mechanisms of the Kagome-like structure under compression and bending load are estimated based on elementary mechanics of materials, and the optimal design is derived in the event that the new structure may serve as the core of a sandwich panel with two face sheets on the top and bottom. The performance of the structure is evaluated in comparison with that of truss PCMs currently available. This new structure is validated against the results of experiments. Moreover, from the results of the compression and bending experiments performed with sandwich panel specimens of three different designs, effects of geometric parameters such as the face sheet thickness and the slenderness ratio of the core struts are analyzed with respects to not only load capacity-per-weight but also the failure mechanisms and the behaviors after a peak load.

2. Analytic solutions and optimization

2.1. Quasi Kagome truss

This study suggests a ‘quasi Kagome truss’, which has a structure similar to the ideal Kagome truss and can be continuously produced through expanded-metal process. Fig. 2 shows a layer of the quasi Kagome truss, which is compared with that of an ideal Kagome truss. On the top of Fig. 2, angled views of the two trusses are illustrated, where the struts located on the upper and lower faces are represented by dashed lines to highlight the struts serving as

the core of a sandwich panel. The unit cell of an ideal Kagome truss shown on the bottom of Fig. 2a has two tetrahedrons, which are connected at one point in the middle, facing each other. When the unit cell is viewed from the top, the triangles lying on the upper and lower surfaces look like they are turned upside down to each other. Like the unit cell in an ideal Kagome truss, that in the quasi Kagome truss has two tetrahedrons facing each other (See the bottom of Fig. 2b). However, there is a subtle difference in the shape of the unit cells; that is, all the struts have exactly the same lengths in the unit cell of the ideal Kagome, while one strut is a little shorter than the remaining two struts in the tetrahedron of the quasi Kagome. The relative density of the quasi Kagome is four times of that of the ideal Kagome. This is manifested in the top views illustrated in the middle of Fig. 2a and b. In other words, the unit cells of the quasi Kagome truss are similar to those of the ideal one, but they are arranged more closely and differently, which might cause a slight increase of the anisotropy in the mechanical properties. However, it has the advantage of cost reduction and higher efficiency of mass-production because it is possible to manufacture the truss core by using well-established press working technologies.

Fig. 3 indicates the final shape of unit cell of the quasi Kagome truss fabricated through the process which will be described in the Section 3.2, where the angles, θ and α , are fixed as 60° in this work. Then, the length of the shortest strut of the three struts composing the upper or lower tetrahedron-like structure, L_{c1} , is related to those of the other two, L_{c2} by $L_{c1} = \frac{\sqrt{3}}{2}L_{c2}$. The width of the shortest strut, b_1 , is designed to larger than those of the others, b_2 , as $b_1 = \sqrt{3}b_2$ so that the axial stresses acting in all the struts may be equalized under a compressive load, P . This design provides another benefit; that is, the axial stresses are also equalized under a shear force, Q , applied in the direction shown Fig. A1 in Appendix A. This new structure has been named the ‘E&B Kagome’ after Expanding and Bending processes.

2.2. Analytic solutions

To estimate the mechanical properties of a sandwich panel with the E&B Kagome core, the equations based on elementary mechanics of materials are derived as follows. It is assumed that the E&B Kagome is composed of ideal struts connected with ball joints. First, regarding the core as a homogeneous material, the equivalent normal yield stress, σ_y^c , and the equivalent shear yield stresses, τ_y^c , of the core are given as follows;

$$\begin{aligned} \sigma_y^c \Big|_{\text{elasticbuckling}} &= \frac{\sqrt{3}\pi^2 E b_2 t_c^3}{6L_{c2}^4}, \\ \sigma_y^c \Big|_{\text{yielding}} &= \frac{2\sqrt{3}b_2 t_c \sigma_o}{L_{c2}^2}, \\ \tau_y^c \Big|_{\text{elasticbuckling}} &= \frac{\pi^2 E b_2 t_c^3}{6L_{c2}^4}, \\ \tau_y^c \Big|_{\text{yielding}} &= \frac{2b_2 t_c \sigma_o}{L_{c2}^2}, \end{aligned} \quad (1)$$

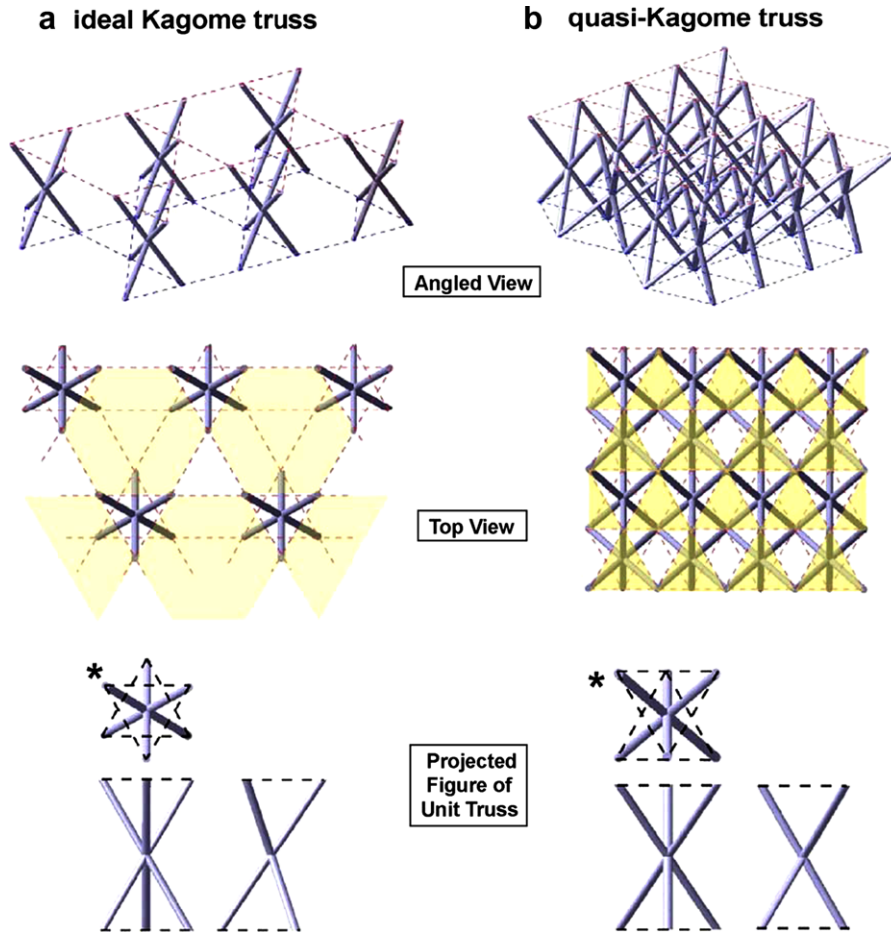


Fig. 2. Configurations of a single layer and a unit cell of (a) ideal Kagome truss compared with (b) quasi-Kagome truss named as E&B Kagome.

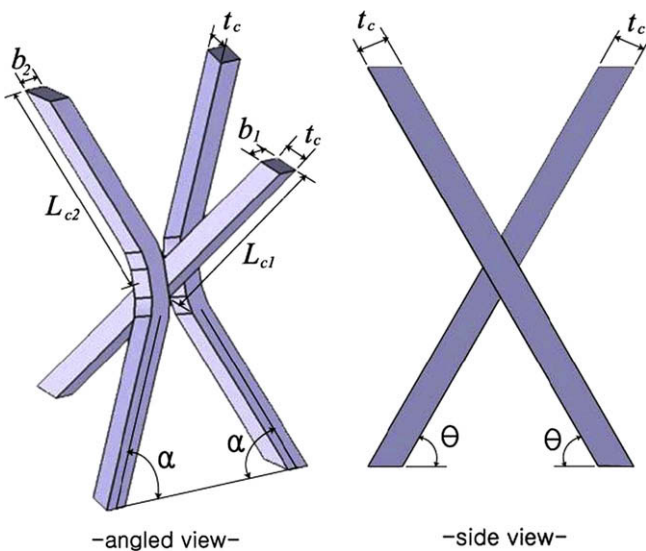


Fig. 3. Configuration of the unit cell of E&B Kagome truss fabricated through forming of a metal sheet.

where σ_o and E are the yield stress and Young's modulus of the raw material, respectively, and t_c is the thickness of the raw metal sheet of the core. Based on two kinds of strut failures, i.e., elastic buckling and yielding or plastic buckling, two different equivalent yield

stresses are defined. A slender member like struts is plastically buckled under compression at exactly the same load level as the yield point if the material has a distinct yield point on its stress-strain curve. For brittle tensile failure, the tensile strength replaces the yield stress, σ_o . It is interesting that the two equivalent yield stresses are related to each other by $\sigma_y^c = \sqrt{3}\tau_y^c$ as if the E&B Kagome core was an isotropic homogeneous material conforming to von-Mises yield criterion. For this reason, the energy approach based on the assumption of homogeneous material of core rather than that based on the direct calculation of forces acting in each strut or face sheet is adopted to derive the equations for the critical load in the following. For the detailed derivation, see Appendix A.

A sandwich panel with a low density core has five different failure modes under a bending load [16], as illustrated in Fig. 4. These modes are as follows: face sheet elastic buckling; face sheet yielding or plastic buckling; indentation; core shear in mode A; and core shear in mode B. For the estimation of the failure loads for each mode, except for face sheet buckling and yielding, two different approaches are available, i.e., the force balance based approach and the energy based approach. The former does not consider either indentation or the difference between the core shear in mode A and the core shear in mode B. And also, the E&B Kagome core is relatively denser than the other truss PCM core so it would be less unreasonable to treat the E&B Kagome as a homogeneous material. Therefore, the energy-balance based approach is adopted in this work. With the equivalent yield stresses of the core given in Eq. (1), the critical loads for the failure modes are expressed as follows: For face sheet buckling (elastic), and yielding or plastic buckling, the load, P_f , is

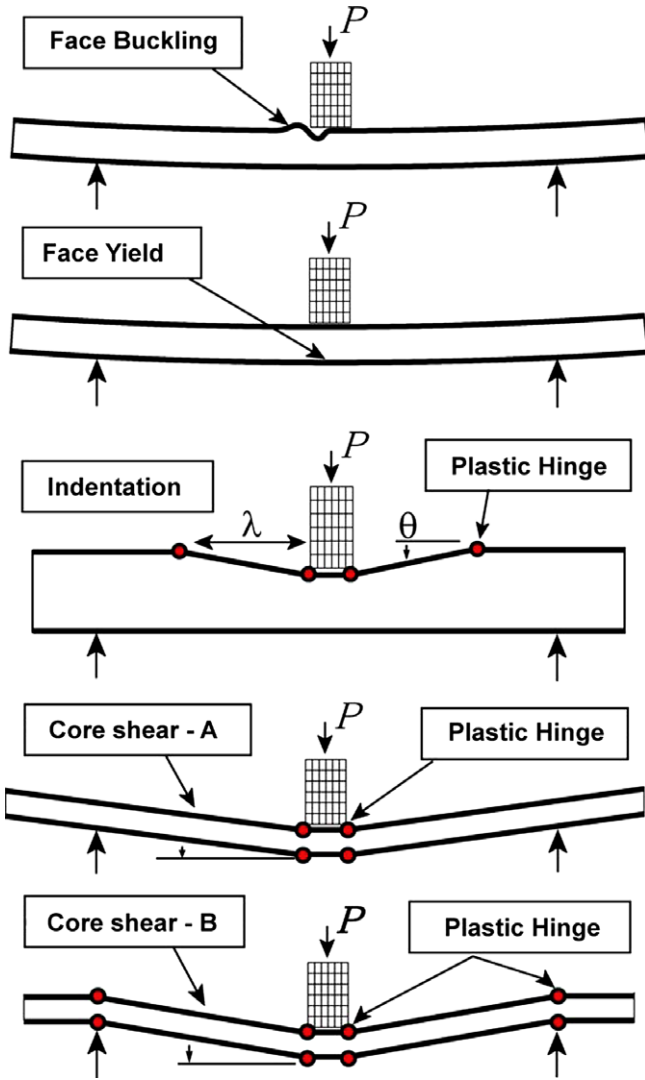


Fig. 4. Failure mechanisms of a sandwich panel with low density core.

$$P_f = \frac{4Bt_f(H_c + t_f)}{S - a} \sigma_y^f, \quad (2a)$$

where $\sigma_y^f = (1 + r^2)^2 \frac{\pi^2 E_f}{12(1 - \nu_f^2)} \frac{t_f^2}{(L_{c2} \sin \alpha)^2} = \sigma_o$.

For indentation,

$$P_I = 2Bt_f \sqrt{\sigma_y^c \sigma_o} + Ba\sigma_y^c, \quad (2b)$$

For core shear modes A and B,

$$P_A = \frac{2Bt_f^2}{S - a} \sigma_o + 2BH_c \left(1 + \frac{2D}{S - a}\right) \tau_y^c, \quad (2c)$$

$$P_B = \frac{4Bt_f^2}{S - 2a} \sigma_o + 2BH_c \tau_y^c, \quad (2d)$$

respectively. These equations are from Ashby et al. [16]. But, considering the finite width of the lower two contact blocks, a , the critical load for core shear in mode B is slightly modified. Also, the first equation corresponding to face sheet elastic buckling is based on the buckling load for a thin sheet of finite width and length given by Ugural [17], where r is the aspect ratio of the truss footstep, L_{s1} , to the width of the panel viewed from the side, B , that is, $r = L_{s1}/B$. If the aspect ratio is low enough, the effect can be ignored.

That is, if $r < 1/3$, $(1+r^2)^2 \approx 1$. In the equations, E_f and ν_f are the Young's modulus and Poisson's ratio of the face sheet, respectively. H_c is the core height, S is the span between the two supporting points, t_f is the face sheet thickness, and D is the overhang. Because there are two kinds of the equivalent yield stresses of the core, σ_y^c and there are two kinds of τ_y^c , too, as shown in Eq. (1), depending on the two kinds of strut failure, each of the last three failure modes has two modes, elastic and plastic. Therefore, there are eight failure modes in total.

2.3. Optimization

In order to derive optimal design of the sandwich panel with the E&B Kagome core, and to evaluate it in comparison with other sandwich panels, the optimization procedure similar to that used by Wicks and Hutchison [5] is used. First, five dimensionless geometric design variables are defined as

$$\vec{x} \equiv (x_1, x_2, x_3, x_4, x_5) = \left(\frac{t_f}{\ell}, \frac{H_c}{\ell}, \frac{t_c}{\ell}, \frac{a}{\ell}, \frac{D}{\ell} \right) \quad (3)$$

where ℓ is the ratio of the maximum moment M to the maximum transverse force V , $\ell = \frac{M}{V}$. Then, the equations for the critical load for the eight failure modes are converted to dimensionless forms shown in Table 1, where the abbreviations of the failure modes are added. In these constraints, there is one dimensionless material parameter, σ_o/E , and there is only one dimensionless load parameter, $\Pi = V/\sqrt{EM}$. Among the six variables, the 4th and the 5th variables regarding the contact block width and the overhang, respectively, are fixed in this work. For a given set of the remaining three variables, i.e., $(x_1, x_2, x_3) = \left(\frac{t_f}{\ell}, \frac{H_c}{\ell}, \frac{t_c}{\ell} \right)$, the dimensionless weight defined as $\Psi = \frac{W}{\rho \ell} = 2 \left(x_1 + \frac{7\sqrt{3}}{2} \frac{x_3}{x_2} \right)$ and the dimensionless loads for the eight failure modes Π are calculated for the following design optimization.

In this work, three kinds of design optimization are presented, where the core thickness, t_c , and the face sheet thickness, t_f , are set to range from 0.1 mm to 3 mm, and the core height, H_c , are set to range from 3 mm to 50 mm. The yield strain is fixed to $\epsilon_y = \sigma_o/E = 0.000837$ for the specimen material used in the experiments, which will be presented in the next section. The first optimization is based on the core height, H_c . Namely, the dimensionless failure load per weight, Π^2/Ψ , is to be maximized for a given H_c under the eight constraints. Fig. 5a and b illustrate failure maps as functions of t_c and t_f for $H_c = 30$ and 40 mm, respectively. The domain boundaries and the contours of failure load per weight, Π^2/Ψ , for the failure modes selected as physically admissible are plotted. A spread sheet code Excel® and a graph software Dplot® were used to generate the maps. In both of Fig. 5a and b, the maximum failure load per weight occurs along the boundary between the domains of the face sheet yielding (FP) and the core shear in mode B plastic (BP) and increases with t_f . In Fig. 5b for $H_c = 40$ mm, it is noted that the domains of the indentation elastic (IE) and the indentation plastic (IP) nucleate between the domains of the face sheet elastic buckling (FE) and the core shear mode-B plastic (BP). To the authors' knowledge, there has been no report showing the indentation in a sandwich panel with PCM cores. In order to check whether the indentation would occur for the corresponding domain in the failure maps of Fig. 5b as it is expected, an example of specimen geometry with $H_c = 40$ mm, $t_f = 0.75$ mm, $t_c = 1.35$ mm, which is marked with the star symbol in Fig. 5b, was used to simulate the deformation behavior under bending load by using the finite element code, ABAQUS of version 6.5. The loading condition at the roller-and-concave-block assembly connected with the upper face sheet (the configuration will be elaborated in the Section 3.3) was simulated as a simple square block. Frictionless contact condition was applied to the contact surfaces between

Table 1
Dimensionless forms of constraints due to several failure modes and abbreviations of the failure modes.

	Elastic buckling		Yielding or plastic buckling	
Face sheet buckling or yielding	$\left(\frac{V^2}{EM}\right) \left(\frac{4(1-\nu^2)}{(1+\nu^2)^2 \pi^2}\right) \frac{x_2^2}{x_1^2(x_1+x_2)} \leq 1$	FE	$\left(\frac{V^2}{EM}\right) \left(\frac{E}{\sigma_0}\right) \frac{1}{x_1(x_1+x_2)} \leq 1$	FP
Indentation	$\left(\frac{V^2}{EM}\right) \left[\frac{3\pi}{2\sqrt{2}} \left(\frac{3\sqrt{3}\sigma_0}{4E}\right)^{1/2} \frac{x_1 x_2^2}{x_2^2} + \frac{27\sqrt{3}\pi^2}{64} \frac{x_4 x_3^2}{x_2^2}\right]^{-1} \leq 1$	IE	$\left(\frac{V^2}{EM}\right) \left(\frac{E}{\sigma_0}\right) \left[\left(\frac{9\sqrt{3}}{2}\right)^{1/2} \frac{x_1 x_3}{x_2} + \frac{9\sqrt{3} x_4 x_3^2}{4 x_2^2}\right]^{-1} \leq 1$	IP
Core shear – mode A	$\left(\frac{V^2}{EM}\right) \left[\frac{1}{2} \left(\frac{\sigma_0}{E}\right) x_1^2 + \frac{27\pi^2}{32} (1+x_5) \frac{x_4^2}{x_2^2}\right]^{-1} \leq 1$	AE	$\left(\frac{V^2}{EM}\right) \left(\frac{E}{\sigma_0}\right) \left[\frac{x_2^2}{2} + \frac{9}{2} (1+x_5) \frac{x_2^2}{x_2}\right]^{-1} \leq 1$	AP
Core shear – mode B	$\left(\frac{V^2}{EM}\right) \left[\left(\frac{\sigma_0}{E}\right) \frac{2x_1^2}{2-x_4} + \frac{27\pi^2}{32} \frac{x_4^2}{x_2^2}\right]^{-1} \leq 1$	BE	$\left(\frac{V^2}{EM}\right) \left(\frac{E}{\sigma_0}\right) \left[\frac{2x_1^2}{2-x_4} + \frac{9x_2^2}{2x_2}\right]^{-1} \leq 1$	BP

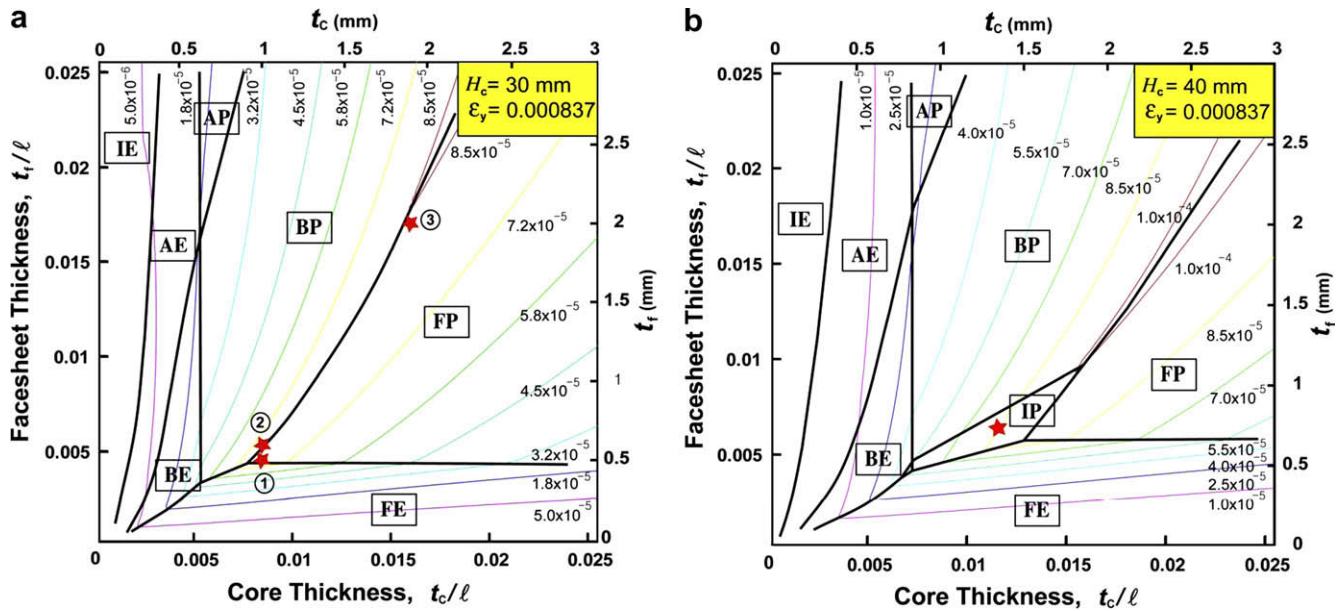


Fig. 5. Failure maps illustrated as functions of t_c and t_f for two given H_c 's. The domain boundaries and the contours of failure load per weight, Π^2/Ψ , for the failure modes selected as physically admissible are plotted; (a) $H_c = 30$ mm and (b) $H_c = 40$ mm.

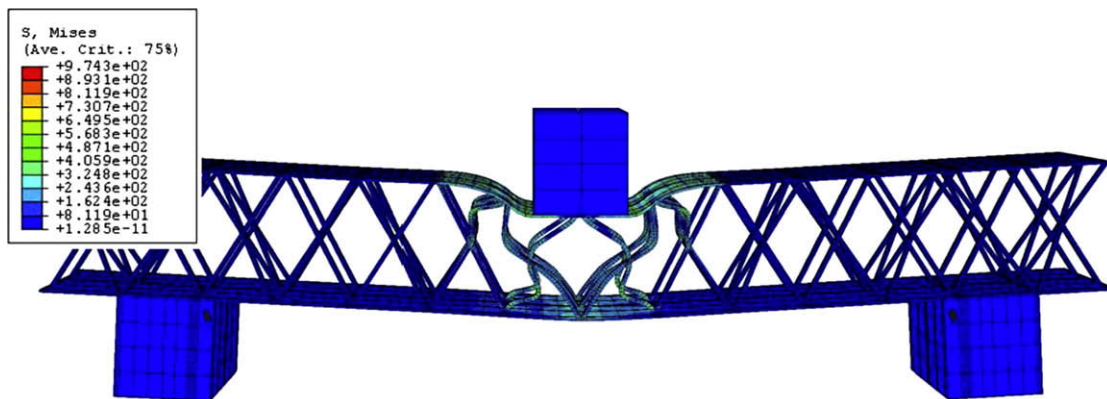


Fig. 6. Deformed shape obtained through finite element simulation for the specimen geometry with $H_c = 40$ mm, $t_f = 0.75$ mm, $t_c = 1.35$ mm, which is marked with the star symbol in Fig. 5b. The deformation vividly indicates that failure was due to the indentation.

the block and the upper face sheet, and the bonding condition using the 'tie constraint' in ABAQUS was applied to the contact surfaces between the face sheets and the core. The 20-node quadratic brick elements and the 15-node quadratic triangular prism elements

were used for the E&B Kagome core and the face sheets, respectively. For the blocks, 20-node quadratic brick elements were used. The total number of elements of the specimen model was 25,216, which was determined after the mesh dependency

check of the computed results. The incremental plasticity theory of isotropic-hardening materials was selected to describe the elastic-plastic behavior of the specimen. As the boundary conditions, the lower blocks and the upper block were modeled to be fixed in the vertical direction and in the horizontal direction, respectively. The simulation results of Fig. 6 show the deformed shape, which vividly indicates that the failure was due to the indentation. From Fig. 5a and b, the maximum performance is found at the high end of the boundaries between FP and BP, and is mostly governed by the face sheet thickness in the ranges of the geometric variables considered in this work.

The second optimization is based on the weight. Namely, the dimensionless load, $\Pi = V/\sqrt{EM}$, is to be maximized for a given weight expressed by Ψ under the eight constraints. The core thickness, $x_3 = t_c/l$, is eliminated from the relation between Ψ and the three variables, so that the maps can be rendered in coordinates $x_1 = t_f/l$ and $x_2 = H_c/l$. Fig. 7 illustrates an example of the failure map for given dimensionless weight, $\Psi = 0.02$. In the figure, a family of constant strength contours is drawn. In ranges of $t_f = 0.1\text{--}1.2$ mm and $H_c = 3\text{--}50$ mm, the failure modes of face sheet elastic buckling (FE), face sheet yielding (FP), indentation plastic (IP), core shear in mode B plastic (BP), and core shear in mode B elastic (BE) occur. In the range of $t_f = 1.2\text{--}3$ mm, the given weight does not yield any physically admissible t_c or H_c . The maximum failure load is achieved at the triple point of face sheet elastic buckling (FE), face sheet yielding (FP), and indentation plastic (IP), where $t_f = 0.75$ mm and $H_c = 43$ mm. Likewise, the specimen geometries, t_f and H_c , could be determined to give the maximum load capacity for various given weights. Fig. 8 shows the maximum failure load capacity, Π_{max} , as a function of weight scale by Ψ . In the figure, the failure modes in which the maximum failure load is achieved are indicated in the abbreviations defined in Table 1. The maximum failure load is mainly found at the triple points of failure modes, but a few exceptions are also found along the boundaries between two failure modes.

The last design optimization is based on the load. Namely, the dimensionless weight, $\Psi = W/\rho l$, is to be minimized for a given load expressed by Π under the eight constraints in Table 1. For a given Π , each combination of dimensions $\{x_1, x_2, x_3\}$ of the entire

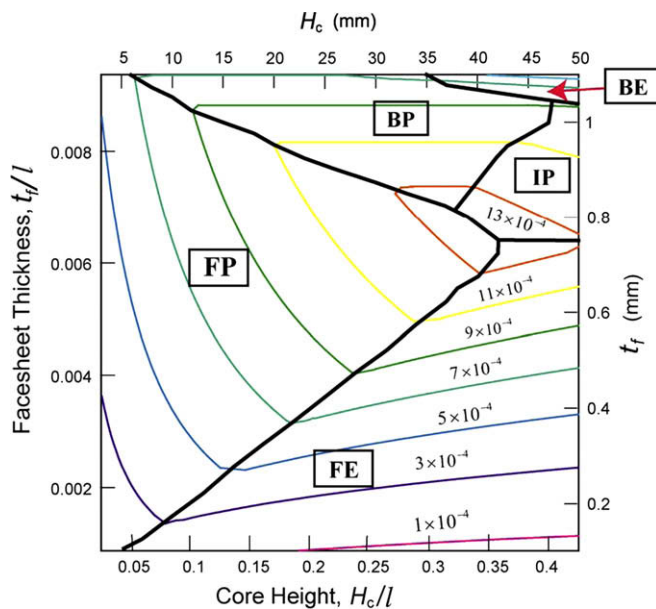


Fig. 7. Dimensionless failure map illustrated as a function of H_c and t_f for a given weight index $\Psi = 0.02$, where a family of constant strength contours of dimensionless failure load, $\Pi = V/\sqrt{EM}$ is plotted.

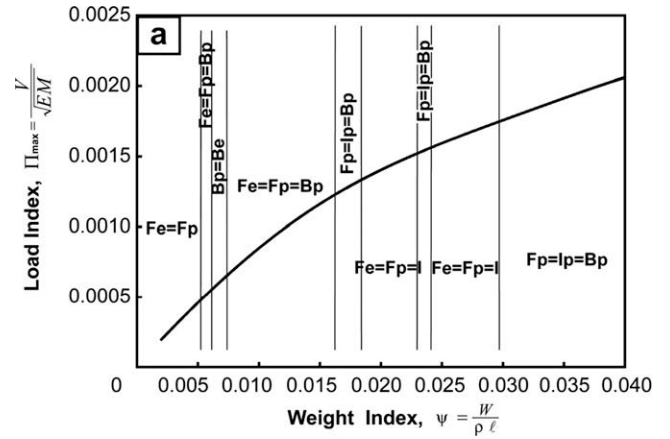


Fig. 8. Maximum of failure load index Π_{max} .

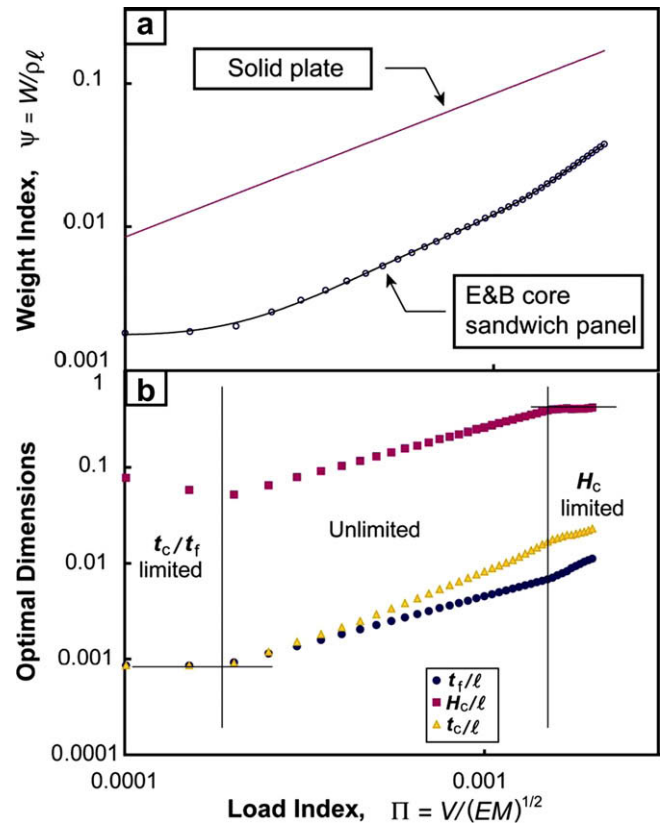


Fig. 9. Variations of (a) Minimum of weight index Ψ_{min} and (b) optimized geometric variables, $x_1 = t_f/l$, $x_2 = H_c/l$, $x_3 = t_c/l$ illustrated as a function of the load index, Π .

space of dimensions considered is tested if it satisfies the eight constraints in sequence, and all the passed combinations are placed into the selected space. Then the weights, Ψ , for the selected combinations are compared to each other to determine the optimal dimension to give a minimum Ψ . Fig. 9a shows the minimum weight, Ψ_{min} , as a function of load, Π , in log–log coordinates. Also, shown for comparison is the weight of a solid sheet of the same material, given in Zok et al. [18]:

$$\Psi = \left(\frac{6E}{\sigma_o}\right)^{1/2} \frac{V}{\sqrt{EM}} \tag{4}$$

Fig. 9b shows the optimal dimensions with the same horizontal axis as in Fig. 9a. While the dimensions are increasing almost linearly in the middle range of the load in log–log coordinates, they are limited by H_c and t_c or t_f , respectively, in the upper and lower ranges of the load. That is, in this optimization process, the core height H_c is set to be no larger than 50 mm. Otherwise, left unlimited, the optimal core height increases monotonically with load capacity, eventually departing the domain of the thin panels. Also, t_c and t_f are set to be larger than 0.1 mm, which is assumed to be the lower limit in practical applications, considering the other panel sizes.

Fig. 10 reveals that the relations between Π and Ψ obtained, respectively, from the last two design optimizations mentioned above agree each other. Namely, the load-based optimization used to obtain the minimum weight yields the same results as the weight-based optimization used to obtain the maximum load capacity. This proves that there is no error in calculation during the two optimization processes.

The mechanical performance of the E&B Kagome cored sandwich panel can be evaluated by comparing the Π – Ψ plot with

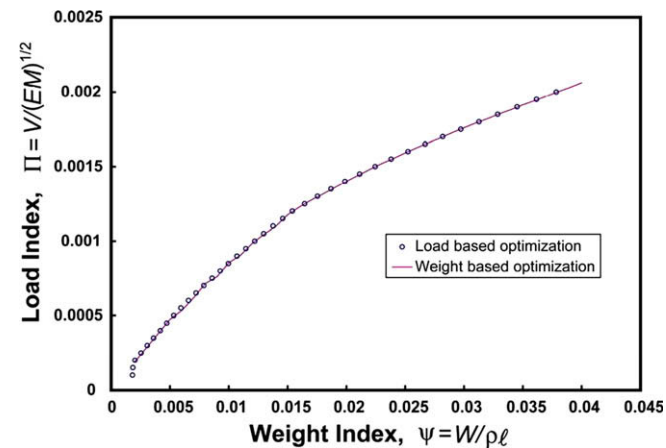


Fig. 10. Two Π – Ψ plots obtained through the load-based optimization and the weight-based optimization.

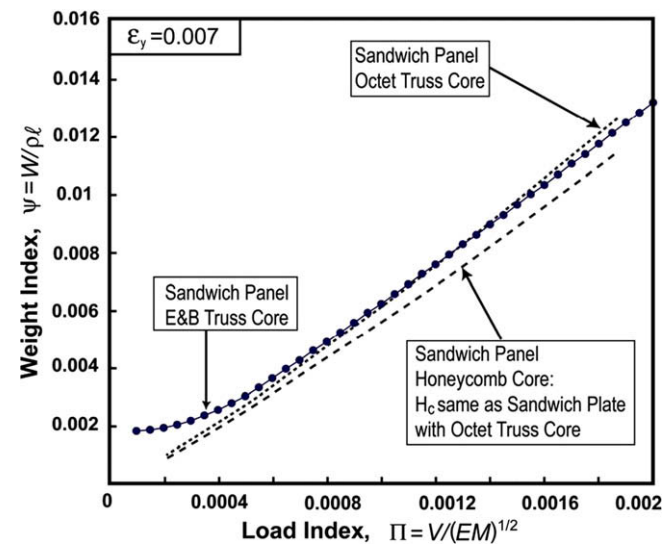


Fig. 11. The performance represented by the Ψ_{\min} – Π plot of the E&B Kagome cored sandwich panel compared with the plots of the octet truss and honeycomb cored ones.

Table 2

Dimensions of three designs of three-point-bend specimen (unit: mm).

Design No.	Face sheet thickness, t_f	Core height, H_c	Truss strut thickness, t_c	Total length, L	Width, B
1	0.5	30	1	344	120
2	0.6		1		
3	2.0		1.85		

those of other sandwich panels. Fig. 11 shows the Π – Ψ plots, where the yield strain is set to $\epsilon_y = \sigma_o/E = 0.007$ and the performance of the sandwich panels with the honeycomb core and octet core are given in Wicks and Hutchison [5]. The E&B Kagome panel performs as good as the octet truss panel, except in the low load region where the weight is overestimated by the lower bound of t_c and $t_f = 0.1$ mm.

3. Experiments

3.1. Specimen design

For case studies, three kinds of specimens were designed as shown in Table 2. These were named Design-1, 2 and 3. All the designs had similar overall sizes, i.e., the total length, $L (=S + 2D) = 344$ mm, the width, $B = 120$ mm, and the core height, $H_c = 30$ mm. Also, all the designs were assumed to be loaded by one three-point-bend jig with span, $S = 265$ mm, contact block width, $a = 30$ mm and overhang, $D = 39.5$ mm. Differences were in the face sheet thickness, t_f , and the thickness of the metal sheet from which the core was fabricated through expanding and bending processes, t_c . The thicknesses of the struts composing the cores, b_1 and b_2 , were given by $b_2 = t_c$ and $b_1 = \sqrt{3}b_2$ in all the designs. These three designs are indicated on the failure map of Fig. 5a. Design-1 is located on the boundary between the face sheet yielding (FP) domain and face sheet buckling (FE) domain, while Design-2 and -3 are located between the face sheet yielding (FP) domain and core shear mode B plastic (BP) domain. Design-3 has much thicker truss struts and face sheets. Nevertheless, the three designs are expected to have the similar level of load-per-weight ratio, Π^2/Ψ .

3.2. Specimen preparation

Both the cores and face sheets were fabricated from sheets of low carbon steel JIS SS41. Because the development of the fabrication process including shearing and expanding machines will be another technical challenge, a simplified approach was taken to fabricate the specimen cores, temporarily. Fig. 12 shows the schematic of the fabrication process. First, a cut of unique pattern was introduced on the sheet by using the YAG laser (Fig. 12a). The sheet was expanded width-wise to be a metal mesh (Fig. 12b). Then, the mesh was bent along the lines connecting the longer ends of the diamond shapes into the corrugated sheet (Fig. 12c and d). Finally, the shorter strut among each of the three struts in the shape of bird foot in the corrugated sheet was rotated 120° in the opposite direction to be the E&B Kagome core (Fig. 12e). All these processes were performed manually. The core was bonded with the upper and lower face sheets by copper brazing (Paste: CTK-C699, CHEM-TECH Korea Co.), which was carried out at 1120°C in the de-oxidation atmosphere of H_2 – N_2 mixture. Fig. 13 shows the microstructure near the brazed joint. The inserts are enlarged optical and SEM (EDX analysis mode) images showing the microstructure near the interface. Well-developed diffusion bonding with minimum defects is observed. Cu component is diffused in the grain boundaries of the mother metal steel.

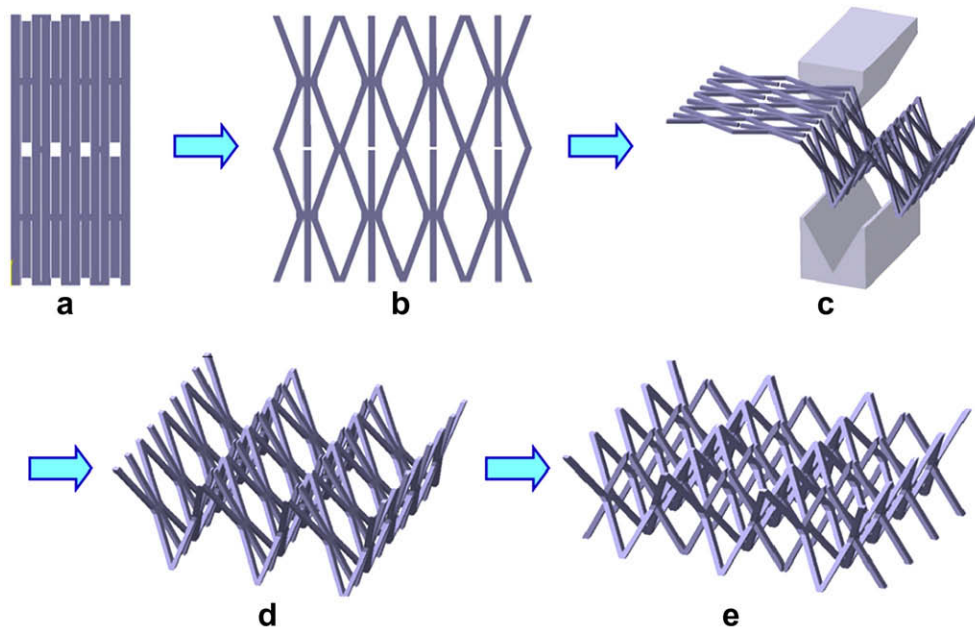


Fig. 12. The schematic of specimen fabrication process; (a) a metal sheet with the cuts of unique pattern introduced by using the YAG laser, (b) a metal mesh obtained by expanding width-wise, (c) bending the mesh along the lines connecting the longer ends of the diamond shapes into (d) the corrugated sheet and (e) E&B Kagome shaped core obtained by rotating the shorter strut among each three struts in a shape of bird foot in the corrugated sheet by 120° in the opposite direction.

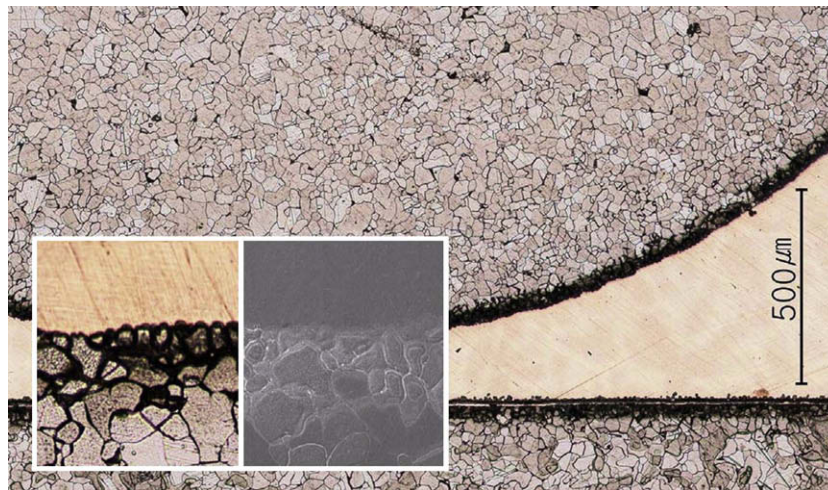


Fig. 13. Microstructure near the brazed joint. The inserts are enlarged optical and SEM (EDX analysis mode) images near the interface.

3.3. Experiments and the results

An electro-hydraulic test machine, INSTRON 8800, was used to measure the material properties of the raw material and to evaluate mechanical performance of the E&B Kagome cored sandwich specimens. For a tension test, a dog-bone type specimen with a 2×2 mm cross sectional area and 40 mm gage length was placed into an electric furnace together with the sandwich specimens and heat-treated under the thermal cycle during the brazing process. Attached with an extensometer, it was tested under 0.002 mm/s displacement control. Fig. 14 shows the stress–strain curve measured by the tensile test. The curve indicates a distinctive yield point followed by unstable deformation. Young's modulus was 203 GPa, and the yield stress and ultimate tensile strength were 170 MPa and 320 MPa, respectively.

Compressive tests were performed with the sandwich specimens of the three designs. Fig. 15 shows the obtained stress–strain

curves. The solid lines denote the equivalent normal yield stress estimated by Eq. (1). For Design-1 and Design-2, which have the same E&B Kagome core, the maximum stresses well agree with the estimated one. For Design-3, the maximum stresses were slightly overestimated. Nevertheless, Eq. (1) yielded fairly good estimation of the equivalent normal yield stress of the E&B Kagome cored sandwich panels.

Three-point-bend tests were conducted with the sandwich specimens of the three designs. Instead of typical roller supports, a roller-and-concave-block assembly was used to suppress the local indentation at the upper face sheet. Displacement was controlled to 0.01 mm/s. The specimen deformation during the tests was monitored by a digital CCD camera. Fig. 16 shows the deformed shapes of the specimens according to Design-1 ~ 3 after the tests. Design-1 specimen failed by the buckling of the upper face sheet, and Design-2 specimen failed by the partial core shear, which seemed to have been triggered a local imperfection of bond-

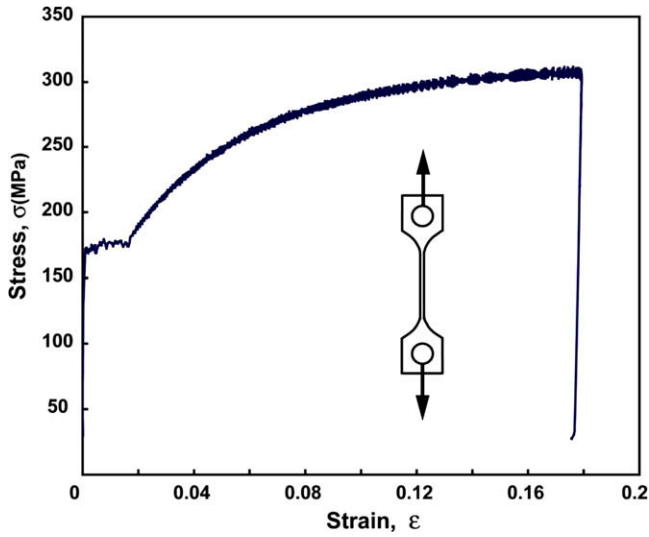


Fig. 14. Stress–strain curve of JIS SS41 steel measured by a tensile test. For the tension test, a dog-bone type specimen with 2×2 mm cross sectional area and 40 mm gage length was placed into an electric furnace together with the sandwich specimens and heat-treated under the thermal cycle during the brazing process.

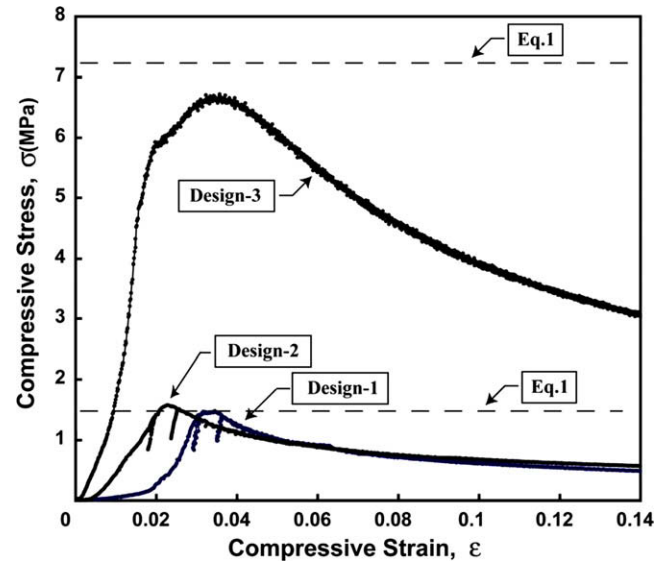


Fig. 15. Stress–strain curves measured by compression tests performed with the sandwich specimens of the three designs. The dashed lines denote the equivalent normal yield stress estimated by Eq. (1).

ing, while Design-3 specimen did not indicate a clear dominant failure mode. Fig. 17 shows the measured load–displacement curves together with those estimated by Eqs. (2a)–(2d). In the curve of Design-1 specimen, the load level sharply dropped at a certain point before a clear yield point was observed. In Design-2 specimen, the curve is similar to that of Design-1, but it showed a yielding point just before the maximum load and then dropped less sharply. On the contrary, in the curve of Design-3 specimen, the load level increased steadily after the initial yield point until P_{\max} , and then decreased slowly. The difference among the load–displacement curves can be interpreted with respect to the nature of the deformations that occurred in the three specimens. In De-

sign-1 specimen, the failure was caused by the elastic buckling of the face sheet; in Design-2 specimen, by the plastic buckling and yielding of the core members accompanied with plastic hinges in the face sheets; but in Design-3 specimen, however, the struts and face sheets were much thicker than those of the rest two designs and very stable plastic buckling and yielding occurred in them, which resulted in the stable failure. Table 3 lists the measured weight and maximum load capacities of the three specimens in comparison with those estimated by the equations described in Section 2.3. In all the designs, the fairly good agreement between the estimated maximum loads with the measured ones demonstrates the accuracy of the approaches taken in this work, even

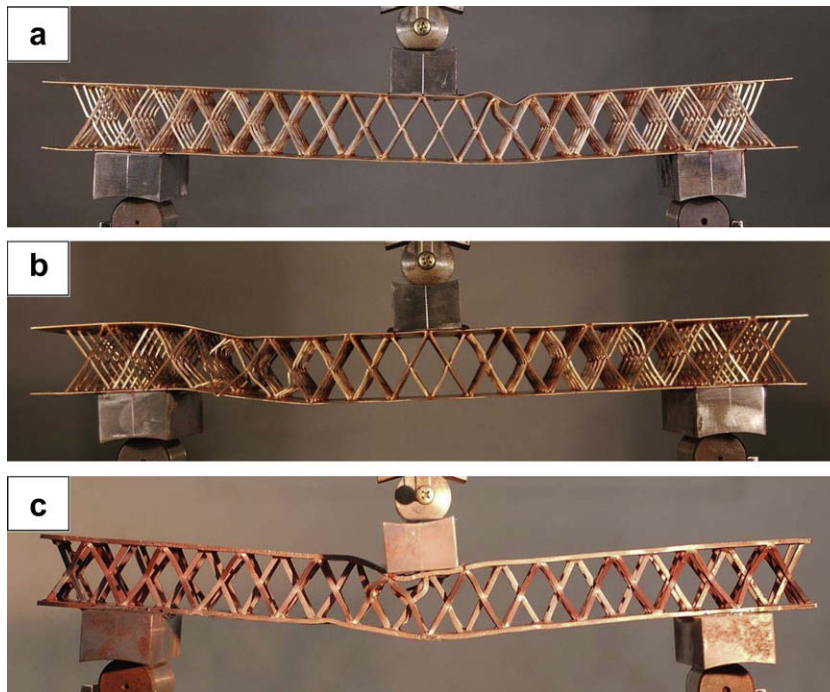


Fig. 16. Deformed shapes of Design-1, 2, 3 specimens after the three-point-bend tests.

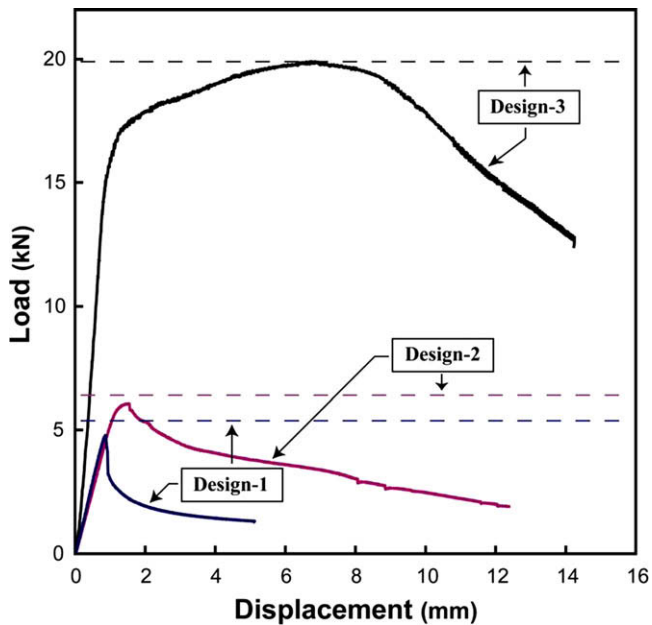


Fig. 17. Load–displacement curves measured during the three-point-bend tests of Design-1, 2, 3 specimens compared with those estimated by Eqs. (2a)–(2d).

though the equations are based on elementary mechanics of materials. The significant differences are found among the maximum load capacities of the three designs, but the load-per-weight ratios are similar to each other. One might say that all the designs have similar performances. However, there is an obvious difference in the performance quality among the designs. That is, Design-1 and Design-2 are substantially inferior to Design-3 in terms of energy absorption and deformation stability after the peak point. No failure at brazed joints were observed until the ends of the compression tests and the bending tests, which proves feasibility of the copper brazing used with the ductile steel of the face sheets and E&B Kagome core.

4. Discussion

In this work, an approach similar to Wicks and Hutchinson [5] has been taken to obtain the optimal designs of the E&B Kagome cored sandwich panel. But, in order to consider a variety of failure mechanisms including face sheet indentation and the different modes of core shear, the equations of constraints (or the failure loads) were derived based on an energy-balance like that in Ashby et al. [16]. It was shown that design of the sandwich panel can be optimized by using a spreadsheet software or a program composed of simple do-loop calculations instead of professional optimization algorithms.

E&B Kagome showed proven performance as cores of sandwich panels under compression and bending load. Compared to the ideal Kagome truss, the E&B Kagome has two more benefits, in addition to those regarding productivity. First, in the E&B Kagome of the

shape to be fabricated, the quasi Kagome trusses are closely packed, and the areal density is four times as high as that of the ideal Kagome. In fact, optimally designed sandwich panels, which are likely to have thin face sheets, often fail due to local indentation by sharp or small objects. For example, highly-concentrated loads, such as from high heels, cause the most floor panel damage of civil airplanes [19]. In the sandwich panels with the ideal Kagome truss core, there are large hexagonal areas on the upper and lower faces that are not evenly supported by the underlying trusses core. See the shadowed area in Fig. 2a. On the contrary, the E&B Kagome core provides even support in uniform regular triangular shape as shown in the shadowed area in Fig. 2b.

Secondly, as mentioned in the Section 2.2, the absolute values of axial stresses acting in the three struts in one E&B Kagome are identical under shear load applied in the direction shown in Fig. A1 as well as under compressive load. This tendency is due to the fact that the force acting in the short strut is related with those in the other two by the same equation, $F_{c1} = 2 \sin \alpha F_{c2}$ under either of the two loads. Even if the width of the struts is not designed as $b_1 = \sqrt{3}b_2$ and if the stresses acting in the three struts are not equalized, the sandwich panel with the E&B Kagome core deforms symmetrically under shear load because every two units of trusses are facing each other in the structure of the E&B Kagome and they are symmetric with respect to the 1–3 plane in Fig. A1 between the two units. See carefully the structures illustrated in Fig. 6 or Fig. 12e. On the contrary, in the ideal Kagome truss or octet truss, the forces acting in the three struts are not identical in magnitude under the shear load applied in the direction of Fig. A1, while they are equal under the compressive load [1,10,20,21]. Furthermore, when the struts fail differently under compression and tensile loads, that is, tensile brittle fracture and compressive buckling, deformation under shear load is inevitably asymmetric in the two opposite directions ($\varphi = 0$ and 180° in Fig. A1). Consequently, under three or four point bending, the sandwich panel with the ideal Kagome or octet truss core deforms asymmetrically with respect to the center loading line when it fails by the core shear modes such as AP, AE, BP, BE. For examples, the sandwich panels with the octet core of beryllium–copper casting alloy [1] and rolled stainless plate [20] have shown the typical asymmetric deformation under three point bending. Therefore, the ideal Kagome or octet truss core has to be designed based on the weak directional shear strength, while the E&B Kagome core does not, because it guarantees symmetric deformation regardless of the width of the struts and the difference of strut failure mechanisms.

For the E&B Kagome to be fabricated at low cost, which is one of the three requirements mentioned above, practical processes for expanding and bending rather than those used for specimen preparation in this work should be developed. New processes based on classical metal forming techniques such as press working have been developed in the authors' laboratory [22].

The expanding and bending processes require the raw metals to have good formability. The authors are considering aluminum alloy 6061 and HSLA (High Strength Low Alloy) steel STDE-100 as candidate metals for future works, which are supported by industries for development of commercial PCMs. Both metals have good form-

Table 3

Measured and estimated performances of the E&B Kagome cored sandwich panel specimens under bending load; weight and maximum load capacities.

Specimen name	Measured			Estimated			Error ($= \frac{B-A}{A} \times 100$)
	Weight (kg)	(A) P_{max} (kN)	$P_{max}/weight$ (kN/kg)	(B) P_{max} (kN)	$\frac{\Pi^2}{\Psi}$	$P_{max}/weight$ (kN/kg)	
Design-1	0.42	4.8	11.4	5.2	7.6×10^{-5}	11.4	8.3%
Design-2	0.48	6.0	12.5	6.3	8.0×10^{-5}	12.1	5.0%
Design-3	1.65	19.8	12.0	22.2	8.5×10^{-5}	12.8	12%

ability for the expanding and bending process when solution-treated or annealed, and they are brazed well by commercial techniques. Moreover, both can be hardened by T-6 aging and quenching, respectively, at a lower temperature than the brazing temperature. Namely, alloy 6061 can be age-hardened at 175 °C to raise the yield stress up to 300 MPa after dip-brazing at 600 °C with Alumibraze® 400 paste [23], and the HSLA steel can be water quenched at 930 °C to raise the yield stress above 1000 MPa after brazing at 1120 °C with copper [24].

5. Conclusions

In conclusion, the new idea suggested for forming a Kagome-like structure based on the expanded-metal process has been proven to be promising with respect to all three requirements, i.e., the morphology, fabrication cost, and raw materials. Three kinds of design optimization were presented, namely, based on the core height, the weight, and the load capacity, respectively. This simple mechanical analysis was effective and accurate enough to estimate the performance of the E&B Kagome cored sandwich panel in comparison with the experimental results. Moreover, through the compression and bending experiments, sandwich panel specimens of three different designs were compared in their mechanical behaviors to demonstrate sensitivity of geometric parameters. Namely, although all the designs had little difference in their load capacity-per-weight, the failure mechanisms and the behaviors after a peak load were totally different.

Acknowledgments

This study was partially supported by Hyundai Motors and by 2006 National Research Lab program of the Korea Science & Engineering Foundation (ROA-2006-000-10249-0). The authors would like to thank Prof. A.G. Evans for initial inspiration and helpful discussion.

Appendix A. Strength of the E&B Kagome unit cell

The lower part of the E&B Kagome unit cell is modeled as a tetrahedron structure as shown in Fig. A1. The strut lengths, L_{c1} , L_{c2} , the truss height, H_c , and the angles, α , θ , γ , are related to each other as follows;

$$\gamma = \theta, \quad H_c/2 = L_{c1} \sin \theta = L_{c2} \sin \alpha \sin \theta. \quad (A1)$$

Under the compressive load applied in the direction-3, Q , according to force equilibrium, the strut forces are given as

$$F_{c1} = -\frac{Q}{2 \sin \theta}, \quad F_{c2} = -\frac{Q}{4 \sin \alpha \sin \theta}. \quad (A2)$$

Under the shear load applied in the direction-2, R , the strut forces are similarly given as

$$F_{c1} = -\frac{R}{2 \cos \theta}, \quad F_{c2} = \frac{R}{4 \sin \alpha \cos \theta}. \quad (A3)$$

If the strut fails by elastic buckling, the buckling occurs first at the longer strut (strut-2) because the critical force is inversely proportional to a square of the strut length according to Euler buckling formula. That is, if the force of the longer strut (strut-2), F_{c2} , reaches to a critical value given as

$$F_{cr,elastic} = \frac{\pi^2 E b_2 t_c}{12 L_{c2}^2}, \quad (A4)$$

the E&B Kagome fails by elastic buckling. However, if the strut fails by material yielding before elastic buckling, all the three struts yield simultaneously because the cross sections of strut-1 and strut-2 are designed based on $b_1 = \sqrt{3} b_2$ to produce the same axial stress

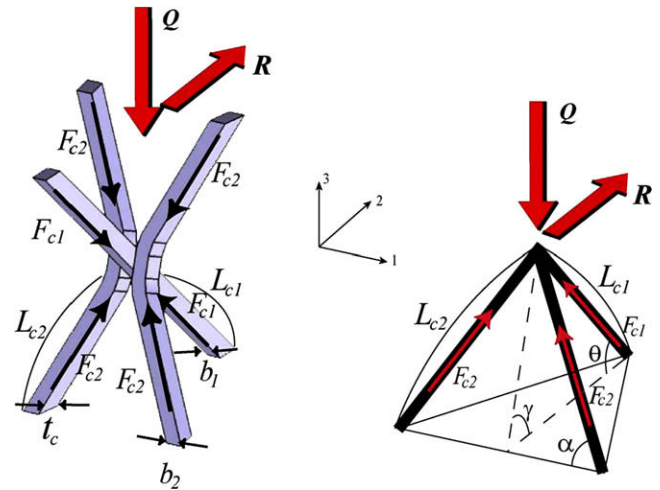


Fig. A1. Configuration of the E&B Kagome unit cell under compressive and shear loads. The lower part is modeled as a tetrahedron structure.

(absolute) under either compression or shear in direction-2. If the force in a strut attains a critical value given as

$$F_{cr,yield} = \sigma_o A_c, \quad (A5)$$

the whole truss fails by yielding or plastic buckling. Here σ_o is the material yield stress, and A_c is the cross sectional area of each strut, that is, $A_c = b_1 t_c$ for strut-1 and $A_c = b_2 t_c$ for strut-2. Therefore, the maximum load under compression, Q_{max} , which the truss can support is determined from Eqs. (A2) and (A4) or Eqs. (A2) and (A5) as

$$Q_{max} = 4 \sin \alpha \sin \theta \times \frac{\pi^2 E b_2 t_c^3}{12 L_{c2}^2} \quad \text{for elastic buckling or} \\ Q_{max} = 4 \sin \alpha \sin \theta \times b_2 t_c \sigma_o \quad \text{for yielding or plastic buckling} \quad (A6)$$

Similarly, the maximum load under shear, R_{max} is determined from Eqs. (A3) and (A4) or Eqs. (A3) and (A5)

$$R_{max} = 4 \sin \alpha \cos \theta \times \frac{\pi^2 E b_2 t_c^3}{12 L_{c2}^2} \quad \text{for elastic buckling or} \\ R_{max} = 4 \sin \alpha \cos \theta \times b_2 t_c \sigma_o \quad \text{for yielding or plastic buckling} \quad (A7)$$

Considering the geometric relations, Eq. (A1), and $\theta = \alpha = 60^\circ$ and the area which the unit cell of truss supports, $A = L_{c1} L_{c2}$, the equivalent normal yield stress, σ_y^c , and the equivalent shear yield stresses, τ_y^c , of the core are given as Eq. (1).

References

- [1] Chiras S, Mumm DR, Wicks N, Evans AG, Hutchinson JW, Dharamasena K, et al. The structural performance of near-optimized truss core panels. *Int J Solid Struct* 2002;39:4093–115.
- [2] Sypeck DJ, Wadley HNG. Cellular metal truss core sandwich structures. In: Banhart J, Ashby MF, Fleck NA, editors. *Proceedings of the second international conference on cellular metals and metal foaming technology (MetFoam 2001)*; 2001. p. 381–6.
- [3] Sypeck DJ, Wadley HNG. Multifunctional microtruss laminates: textile synthesis and properties. *J Mater Res* 2001;16:890–7.
- [4] Deshpande VS, Fleck NA, Ashby MF. Effective properties of the octet-truss lattice material. *J Mech Phys Solids* 2001;49:1747–69.
- [5] Wicks N, Hutchinson JW. Optimal truss plates. *Int J Solid Struct* 2001;38:5165–83.
- [6] Evans AG, Hutchinson JW, Fleck NA, Ashby MF, Wadley HNG. The topological design of multifunctional cellular metals. *Prog Mater Sci* 2001;46:309–27.
- [7] Hyun S, Karlsson AM, Torquato S, Evans AG. Simulated properties of Kagome and tetragonal truss core panel. *Int J Solid Struct* 2003;40:6989–98.
- [8] Hyun S, Torquato S. Optimal and manufacturable two-dimensional Kagome-like cellular solids. *J Mater Res* 2002;17:137.

- [9] Wadley HNG, Fleck NA, Evans AG. Fabrication and structural performance of periodic cellular metal sandwich structures. *Compos Sci Technol* 2003;63:2331–43.
- [10] Wadley HNG. Multifunctional periodic cellular metals. *Philos Trans Roy Soc* 2006;A 364:31–68.
- [11] Wadley HNG. Cellular metals manufacturing. *Adv Eng Mater* 2002;4:726–33.
- [12] Zok FW, Waltner SA, Wei Z, Rathbun HJ, McMeeking RM, Evans AG. A protocol for characterizing the structural performance of metallic sandwich panels: application to pyramidal truss cores. *Int J Solid Struct* 2004;41:6249–71.
- [13] Jung CG, Yoon SJ, Yang DY, Lee SM, Na SJ, Lee SH, et al. Fabrication and static bending test in ultra light inner structured and bonded (ISB) panel containing repeated pyramidal structure. *J Korean Soc Prec Eng* 2005;22:175–82.
- [14] Lim JH, Kang KJ. Wire formed cellular metals. *Mater Trans* 2006;47:2154–60.
- [15] Kang KJ, Lim JH, Nah SJ, Koo MH. Compressive and bending behavior of sandwich panels with octet truss core fabricated from wires. *Trans Korean Soc Mech Eng* 2005;A 29:470–6.
- [16] Ashby MF, Evans AG, Fleck NA, Gibson LJ, Hutchison JW, Wadley HNG. *Metal foams: a design guide*. Butterworth Heinemann; 2000.
- [17] Ugural AC. *Stresses in plates and shells*. McGraw-Hill; 1981. p. 156.
- [18] Zok FW, Rathbun HJ, Wei Z, Evans AG. Design of metallic core sandwich panels. *Int J Solids Struct* 2003;40:5707–22.
- [19] Tsotsis TK, Lee SM. Characterization of localized failure modes in honeycomb sandwich panels using indentation ASTM STP 2174; 1996. p.139–65.
- [20] Rathbun HJ, Wei Z, He MY, Zok FW, Evans AG, Sypeck DJ, Wadley HNG. Measurement and simulation of the performance of a lightweight metallic sandwich structure with a tetrahedral truss cores. *Trans ASME J Appl Mech* 2004;71:368–74.
- [21] Wang J, Evans AG, Dharmasena K, Wadley HNG. On the performance of truss panels with Kagome cores. *Int J Solids Struct* 2003;40:6981–8.
- [22] Yoon CS, Jeong JG, Kang KJ, Lim CH, Park MS. Device for method for manufacturing expanded metal for sandwich panel. Korea Patent; 2007, No. 10-0706375.
- [23] Lee YH. Mechanical behaviors of bulk Kagome truss PCMs woven of metal wires. Master Thesis. Chonnam National University; 2007.
- [24] Lim CH. Design and manufacture of ultra light metal structures using expanded metal. Master Thesis, Chonnam National University; 2007.